Beachrock: A tool for reconstructing relative sea level in the far-field

Barbara Mauz [a,*], Matteo Vacchi [b], Andrew Green [c], Goesta Hoffmann [d], Andrew Cooper [c,e]

[a] School of Environmental Sciences, University of Liverpool, Liverpool L69 7ZT, UK
[b] Aix-Marseille Université, CEREGE CNRS-IRD UMR 34, Aix en Provence, France
[c] School of Agriculture, Earth and Environmental Sciences, University of KwaZulu-Natal, Private Bag X54001, Durban, South Africa
[d] German University of Technology in Oman, P.O. Box 1816, Athaibah PC 130, Oman
[e] School of Environmental Sciences, University of Ulster, Coleraine BT52 1SA, UK

A B S T R A C T

Today's understanding of sea-level change developed through a combination of process-based physical modelling and observational data. Observational data of sea-level change derives from coral reefs in the far-field of the former ice sheets where a geographically variable relative sea-level signal is expected as a response of the earth to ocean loading. Given this variability and the limited geographical distribution of coral reefs, there is a need to explore other, non-coral based sea-level markers to further understand sea-level change and, for example, to 'fingerprint' melt-water. Here, we present beachrock as a coastal deposit suitable for relative sea-level (RSL) observations in the far-field. Beachrock is an intertidal deposit forming in the zone where carbonate saturated meteoric and marine water mix and pCO_2 decreases. We provide the conceptual framework for beachrock analysis and describe techniques suitable for analysing and dating the deposit. The approach is standardised by outlining the sediment characteristics in terms of RSL indicative meaning and indicative range, and is tested against published data. A study conducted on coasts of the Mediterranean Sea exemplifies the utility of beachrock for RSL reconstruction. It is shown that the precision of the reconstruction is derived from the combined uncertainty of age and tidal amplitude or tidal range. The uncertainty can be reduced to half the tidal amplitude when a deposit can be ascribed to the upper (or lower) intertidal zone. Beachrock-based data benefit from the lack of non-quantifiable error terms such as post-depositional compaction due to the instantaneous formation and high preservation potential of the deposit. This underlines the high precision of beachrock-based RSL reconstruction, which is a prime requirement for testing and extending coral-based records.

© 2015 The Authors. Published by Elsevier B.V. This is an open access article under the CC BY-NC-ND license (http://creativecommons.org/licenses/by-nc-nd/4.0/).

1. Introduction

Observational data from many coasts around the world indicate that sea level is rising with difficult consequences for low-lying coasts (e.g., Nicolls and Cazenave, 2010). Extrapolation into the future suggests moderate sea-level rise, however, there is a high degree of uncertainty, in particular at the regional scale (Gehrels and Long, 2008). Informed decisions at a regional scale are highly dependent on precise sea-level projections, which improve the longer the regional relative sea-level (RSL) curve stretches back into the past. During the last deglaciation the sea level rose with both fast and slow velocities; a regional RSL curve that covers the last deglaciation therefore improves our understanding of the regional coastal response to various forms of sea-level rise.

In the far-field of the former ice sheets the relative sea-level signal varies due to the variable response of the earth to ocean loading. While the physics of this spatial variation is well understood (Mitrovica et al., 2010), the effect of the mechanisms on a regional scale is poorly constrained due to insufficient observations over wider areas in the far-

field. While coral reef deposits are excellent RSL markers, the vertical living range of the coral species is large and their growth rate is not linear (Montaggioni, 2005). There is therefore a need to find alternative RSL markers that can be used to test the coral-based records from Tahiti and Barbados and to establish records where no coral markers are available (e.g., Livsey and Simms, 2013).

One such marker is beachrock, a littoral deposit occurring predominantly in the far-field that is lithified almost instantaneously and thereby records the position of the corresponding shoreline (Hopley, 1986). Many workers have studied the deposit and Vousdoukas et al. (2007) provided a comprehensive overview on formation, occurrence and relevant literature. After the early description of Stoddart and Cann (1965), the properties suitable for RSL reconstruction were first highlighted by Hopley (1986), but, in comparison to other RSL markers, beachrock remained understudied. Here, we highlight the properties of beachrock that are useful for RSL reconstruction and quantify associated uncertainties. We aim at providing the basic methodology for increasing the number of observational data in mid-latitudinal and far-field regions and at standardising the scientific approach of using beachrock as a RSL indicator. Using an example, we show how the beachrock can be transformed into a sea-level index point (SLIP) with well-defined

indicative meaning and tidal datum. We discuss the potential and limitations of the approach in the light of our own results and other published data.

2. Beachrock: sea-level related characteristics

Beachrock is a lithified coastal deposit where lithification is a function of CO_3^{-2} ion concentration in seawater, microbial activity and degassing of CO_2 from seaward flowing groundwater. Field experiments (e.g., Hanor, 1978) and coastal observations (e.g., Hopley, 1986) suggest that cementation occurs within a few decades where suitable coastal morphology provides sufficient accommodation space for soft sediment to settle.

2.1. The sediment

Sediment that is suitable for transformation into rock on a decadal time scale needs to provide sufficient pore space for carbonate crystals to precipitate and grow. Typically, its texture is coarse silt to sand, sometimes with pebbles. The rate of sediment supply must be limited in order for the diffusive transport of CO_2 through overlying sediment to be effective (Hanor, 1978) and for the carbonate factory to operate without perturbation. The cementation rate must therefore outpace the sedimentation rate for the rock to form.

Beachrock has sedimentary textures and bedding structures indicative of the upper shoreface to beach sedimentary environment where shoaling waves and longshore currents operate. The upper shoreface to foreshore environment is typically characterised by small asymmetrical ripple foreset laminae (Fig. 1A), low angle laminar or foreset beds dipping seaward (Fig. 1B) or by horizontal plane-parallel laminar beds, depending on the dip of the shore profile and flow criticality (see also Bezerra et al., 1998). Between the wave-breaker surf zone and swash and back-wash zone a lag deposit may form. Towards land symmetrical ripples and horizontal bedding characterise the foreshore

zone (Fig. 1C). These structures vary depending on the morphology of the coast and its tidal and wave regime (e.g., Vieira et al., 2007).

The thickness and lateral extent of a beachrock deposit depends on both sediment supply and accommodation space. Thin (<2 m) and probably isolated beds form in pockets on reflective, bedrock-controlled coasts; these beds are larger on intermediate and dissipative coasts. Beachrocks may preserve antecedent morphologies such as coastline-parallel ridge and runnel-type features.

2.2. The cement

The cement by which the loose sand is locked into position is indicative of the nearshore zone between shoreface and beach, at the interface between seawater and meteoric water (Fig. 2). The interface is the mixing zone, the chemically most active zone, where beachrock forms. The zone is characterised by a pore fluid that is a mixture of different end-member solutions (Moore, 1973), originating from the adjacent environments (e.g., hypersaline waters from sabkhas; meteoric water from groundwater). The chemical characteristics of the solutions, in particular acidity and under- or supersaturation with respect to calcite, control the precipitation of the carbonate mineral when the initial pCO_2 falls due to degassing (Plummer, 1975; Meyers, 1987). As a carbonate mineral will only precipitate from a solution that is supersaturated with respect to this mineral, the mixing of the groundwater and seawater must result in supersaturation. Plummer (1975) showed that for this to happen the mixture must contain more than 50% seawater, the end-member solutions are in equilibrium with calcite and the pCO_2 drops below 10^{-2} atm (Fig. 3A). The higher the temperature, the less seawater is required to achieve supersaturation (Fig. 3B) and the more CO_2 escapes, the higher the pH and the faster carbonate minerals can precipitate. Thus, the sediment layer that is closest to the water table will cement first and fastest and preferred areas of the layer are those where microbes are active (Neumeier, 1998). If the end-member solution contains Mg^{2+}, high magnesian calcite (HMC) precipitates and the typical crystal form of this mineral is bladed or granular

Fig. 1. Examples for sedimentary bedding structures of beachrock deposits. A — cross-bedded beachrock at the seaward end of beachrock deposit at 1 m water depth. Tidal range is around 0.2 m (Naxos Island, Mediterranean Sea, 37,09° N 25,36° E; see hammer of 35 cm length for scale); B — low angle trough cross bedded foreset beds dipping seaward (above dashed black line); C — horizontal bedding (below dashed black line) and planar forest beds. Each sediment package is around 25 cm thick.
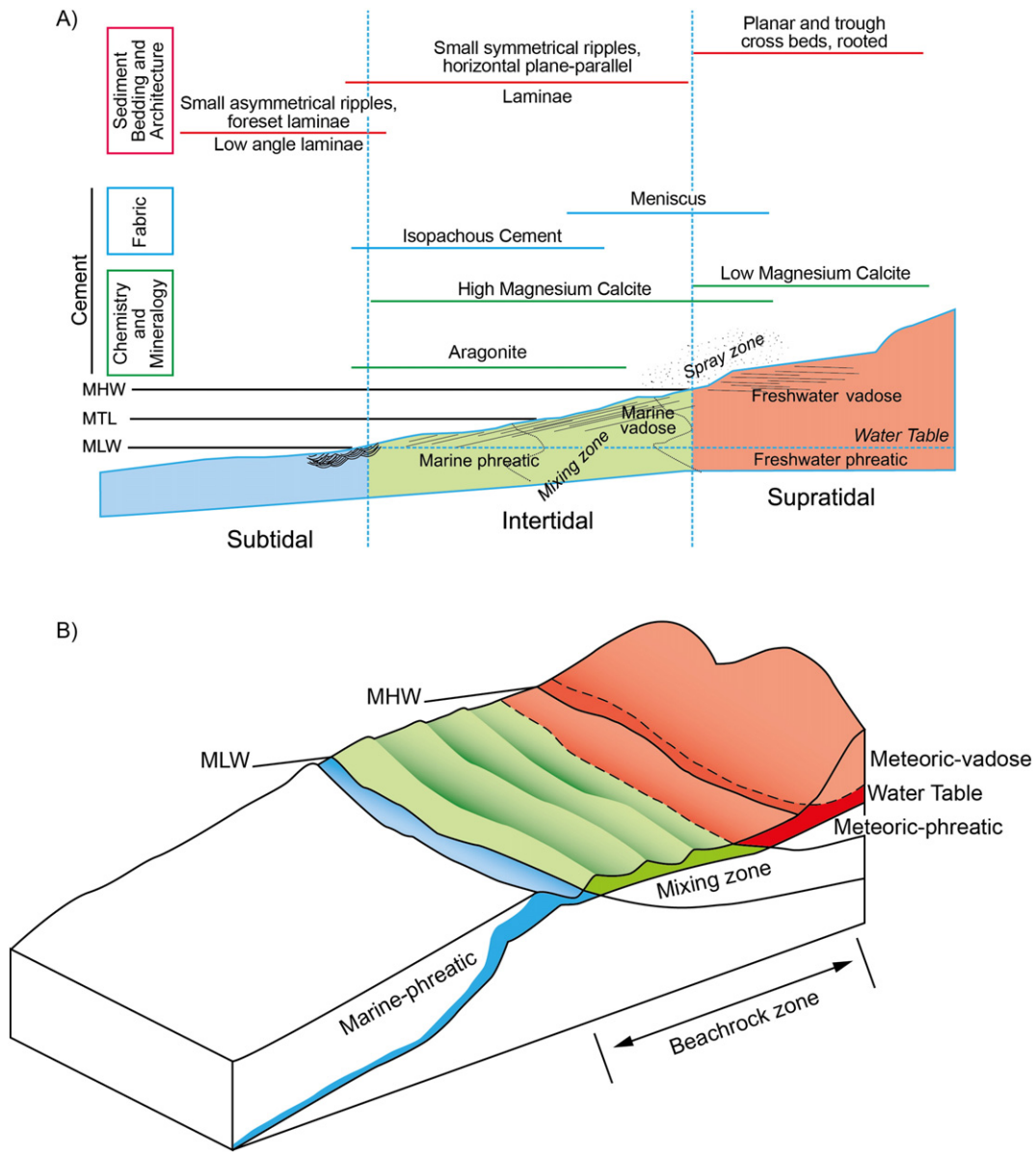
Fig. 2. Schematic illustration of the coast and its zones of cement fabrics, preferred carbonate geochemistry and sediment bedding structures; A — 2D illustration; B — 3D illustration. Beachrock forms in the mixing zone which includes the marine-vadose and the marine-phreatic environment.

(Fig. 4A) or it is micritic when microbes are involved in the precipitation (Neumeier, 1998). The higher the temperature of the solution, the faster aragonite precipitates relative to calcite (Burton and Walter, 1987) and the crystal form the cement takes is mostly fibrous (Fig. 4B). Crystal arrangement and fabric is controlled by environment and gravitation. HMC and aragonite form circumgranular rim in meniscus fabric in the vadose environment (Fig. 4C) or symmetrical crusts in the meteoric environment. In most beachrocks the pore space is not completely occluded but is filled with mosaic fabric and may remain empty in the centre. Fig. 2 depicts the spatial relationship between carbonate cementation zones and Table 1 provides the details of the cement types in terms of crystal form, size and fabric.

Diagenesis takes place in the subsurface in response to a change in water-table elevation, temperature or pressure. Diagenesis involves processes such as dissolution, reprecipitation and recrystallisation and the end-point of these processes is chemical stability. The process follows the relative thermodynamic stability of magnesian calcite and aragonite and the chemistry of the pore fluid. The thermodynamic

calculations reveal the metastability of aragonite with respect to calcite, and of magnesian calcite with respect to calcite and dolomite (Morse and Mackenzie, 1990). Most effective in terms of creating the end-members calcite and dolomite is the infiltration of meteoric water depleting the cement in Mg, Sr and Na and enriching it with other elements (e.g., Fe^{2+}). Dissolution and subsequent creation of secondary porosity can occur through infiltration of meteoric water where the dissolution capacity of the water is largely controlled by the amount of dissolved CO_2 and the permeability of the arenite frame resulting often in moulds and vugs. These can be later filled with marine cement or intraclasts.

The pathway of the diagenetic process is influenced by the original composition of the sediment. For example, coralline algae colonising the foreshore of many coasts, has the highest $MgCO_2$ content of all coastal magnesian calcite components (7–20 mol% $MgCO_3$; Milliman et al., 1971) and is the least susceptible to replacement by calcite (Walter and Hanor, 1979). In the Mediterranean calcite cement in algae has about 15 mol% MgCO3 and this cement is petrographically
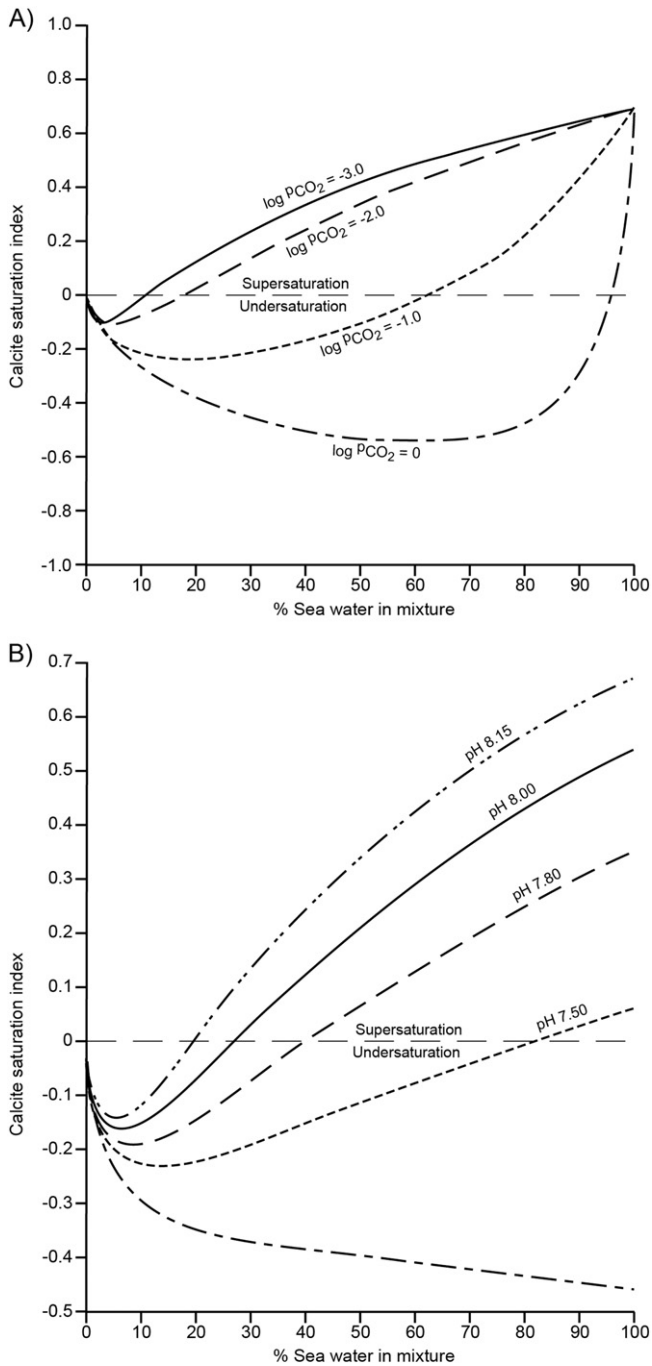
Fig. 3. Geochemical characteristics of the intertidal mixing zone. The saturation index was calculated using a chemical model which considers ion-activity coefficient and thermodynamic data at 25 °C for the most important inorganic ions (e.g., Mg, Na, K) and ion pairs in solution (Plummer, 1975). A — calcite saturation index for mixtures of solutions that were saturated with calcite at different pCO_2 at pH of 7.5; B — calcite saturation index for mixtures of solutions that were in equilibrium with calcite at $10^{-2.5}$ atm.

Fig. 4. Various cement types forming in the intertidal mixing zone. A — isopachous rim cement composed of microcrystalline HMC; B — small calcite crystals filling pore space in granular fabric; C — bladed aragonite crystals growing normal on surface of quartz grains.

identical to beachrock cement in many regions (Alexandersson, 1985). HMC is thus the likely cement where red algae constitute part of the coastal sediment.

The diagenetic process can be reversed under the presence of foreign substances (e.g., orthophosphate from an overlying soil; Walter and Hanor, 1979) which changes the relative stability of the three carbonate minerals and thereby impacts on the preferential dissolution of one or the other carbonate mineral. The process can also be delayed, in particular in the presence of Mg, because geochemically, Mg^{2+} ions function

as an inhibitor of carbonate precipitation. The less Mg the pore fluid contains, the larger calcite crystals and the less fragile the rock.

The burial history is thus characterised by cement phases and these phases can constitute compositional zoning (Meyers, 1974) on surfaces of components and in pore spaces. It is important to identify this zoning, mostly represented by carbonate fringes and granular mosaics, because diagenesis can obscure the beachrock origin and thus overprint its usefulness as a RSL indicator.

2.3. Preservation

The degree of preservation depends on the rate of sea-level change and the rate of lithification where the latter must exceed the rate of

Table 1
Typical primary cement types and fabrics in beachrock. Listed are crystal form and orientation of c-axis on surface of components and in pore space in comparison to the water from which they precipitate, fabric of crystal assemblage, chemistry of precipitate and CL colours.

Environment	Water	Grain Surfaces	Pore Space	Fabric	Chemistry/Mineral	CL
Upper beach	Unmixed groundwater	Scalenohedral to rhombohedral (dog tooth), normal orientation	Equant subhedral, crystal size >30 μm; random orientation	Drusy to blocky, gravitational, syntaxial overgrowth	LMC or HMC	Blue
Lower beach to upper foreshore	Mixed water	Bladed, fibrous, normal orientation	Granular, crystal size 30 μm or empty	Gravitational, mosaic, syntaxial overgrowth	HMC	Subdued blue, violet
Lower foreshore to upper shoreface	Sea water	Microcrystalline, fibrous	Often empty, or granular	Symmetrical around grains	HMC, aragonite	orange
Lower shoreface	Sea water	Microcrystalline, fibrous	Empty, micrite (below fair-weather base)	Symmetrical around grains	HMC, aragonite	Bright orange

RSL change. Field observations suggest years to decadal time scales for cementation (Vousdoukas et al., 2007) and experimental evidence suggests fastest lithification from beach groundwater (Hanor, 1978) where larger crystals bind components. With increasing sea-water mixing the process is slower (Hanor, 1978); smaller carbonate crystals alongside high porosity make the rock more friable on the seaward side of the deposit. Under constant hydrodynamic conditions the landward part of a beachrock bed is therefore better preserved while its seaward part may be reworked under changing wave energy. We consider two types of reworking: synsedimentary and postsedimentary. As cementation is so rapid, contemporaneous reworking (e.g., by storm surge) is easily identified through intraclasts, which become part of the deposit immediately after a high-magnitude event. If such an event occurs after deposition, parts of the deposit are displaced and deposited as boulders downdip or updip of the storm surge trajectory.

3. Suitable analytical techniques

Several standard techniques apply to beachrock analysis. These include: surveying to estimate elevation, mapping and logging to identify macroscopically lateral facies relationships and thin section-based petrographic microscopy to identify the depositional environment including the type of cement. Here, we highlight other suitable sediment analysis techniques less used in beachrock analysis and outline the two most suitable dating and surveying techniques.

3.1. Surveying, mapping and sampling

On land, the elevation of the deposit can be surveyed using high-precision instruments, such as differential GPS, which can measure with vertical precision of few decimeters or better (Casella et al., 2014; Rovere et al., 2014). Other survey methods can be employed, such as triplometers or hand levels, but these provide lower precision and must be evaluated through repeated measurements and benchmarked against a tidal datum.

A yet to be explored number of beachrock deposits occur below modern mean sea level. Side Scan Sonar, multibeam and echosounding datasets can be supported by direct SCUBA diving techniques to map and to sample beachrocks down to around 30 m water depth (e.g., Antonioli et al., 2007; Desruelles et al., 2009; Vacchi et al., 2012a). The exact water depth is recorded by averaging 2 electronic depth gauges with a precision of 0.5 m (at depths ≥ 3 m; Rovere et al., 2010). In shallower water, precise measures can be obtained using a metal bar with a precision ≤ 0.5 m (Vacchi et al., 2012b).

3.2. Ground penetrating radar

Ground Penetrating Radar (GPR) is a fast, non-destructive and non-invasive geophysical method used for high-resolution mapping of the shallow subsurface. The method relies on short pulses of high frequency electromagnetic energy transmitted into the ground by a transmitting antenna. There, the waves are reflected in zones of contrasting material properties. The reflected waves are received by the system and the two-way travel time is recorded. The penetration depth of the radar-waves depends on the sediment, the water content and the antenna frequency where the frequency of the radar waves and the resulting resolution are positively correlated. The vertical resolution is in the range of a few centimetres and the penetration depth may be tens of metres and drops with higher frequencies. A 2D-cross section (radargram) is generated while moving the system along a line. The radargram reveals layer boundaries and sedimentary structures essential for correlation between outcrops and mapping of the stratigraphic architecture. Limitations of the method are high electrical conductivity in the subsurface (e.g., due to sea water intrusion) and fine-grained sediments (silt, clay) that reduce the penetration depths. GPR surveys on sandstones and other hardrock are a common procedure, whereas GPR surveys on beachrock (Fig. 5) have rarely been performed. Davis and Annan (1989), Bristow and Jol (2003) and Neal (2004) provided a general overview of this and Koster et al. (2014) described the use of GPR in an arid coastal setting. As beachrocks are relatively thin deposits, high frequency antennas (400 MHz or higher) are appropriate for the scale of resolution required. Uplifted coastal areas where the beachrock is situated above the water table are prime targets for GPR surveys.

3.3. Cathodoluminescence

This technique is a tool to identify type and zonation of the cement. The luminescence is a function of the relative concentration of Mn^{2+} as the primary activator ion and Fe^{2+} as the deactivator ion. Its intensity is controlled by the absolute amount of Mn^{2+} concentration, by the Fe/Mn ratio in calcite (Hemming et al., 1989) and by rate of crystal growth (Ten Have and Heijnen, 1985). The colours are visually categorised as bright, moderate, dull and non-luminescent. The early precipitation of carbonate cement is from oxidising pore water and this water is free of Mn and Fe so that the first zone is non luminescent. When the water begins to stagnate, Mn-bearing carbonate minerals precipitate and these emit yellow to red colours. The intensity of these colours is a function of the reducing conditions of the pore water and the extent to which Fe is exported. Thus, marine cement is virtually non-luminescent due to the positive Eh of sea water and changes to yellow-orange colours when the cement precipitates from more Eh-negative waters (Fig. 6). The spatial mix of colours may indicate repeated dissolution and precipitation phases cutting across crystal tops and isolation zones of earlier versus later cementation. Amieux et al. (1989) studied tropical beachrock and found primary cement of isopachous fibrous aragonite rim emitting very dull orange and blue colour; the pores were filled by equant crystals emitting a bright yellow-orange colour and larger equant crystals emitting dull blue and medium orange colours. The zonation was interpreted as indicating a progression from a marine to a freshwater environment, characterised by early marine cementation and subsequent early diagenesis in mixed water followed by freshwater.
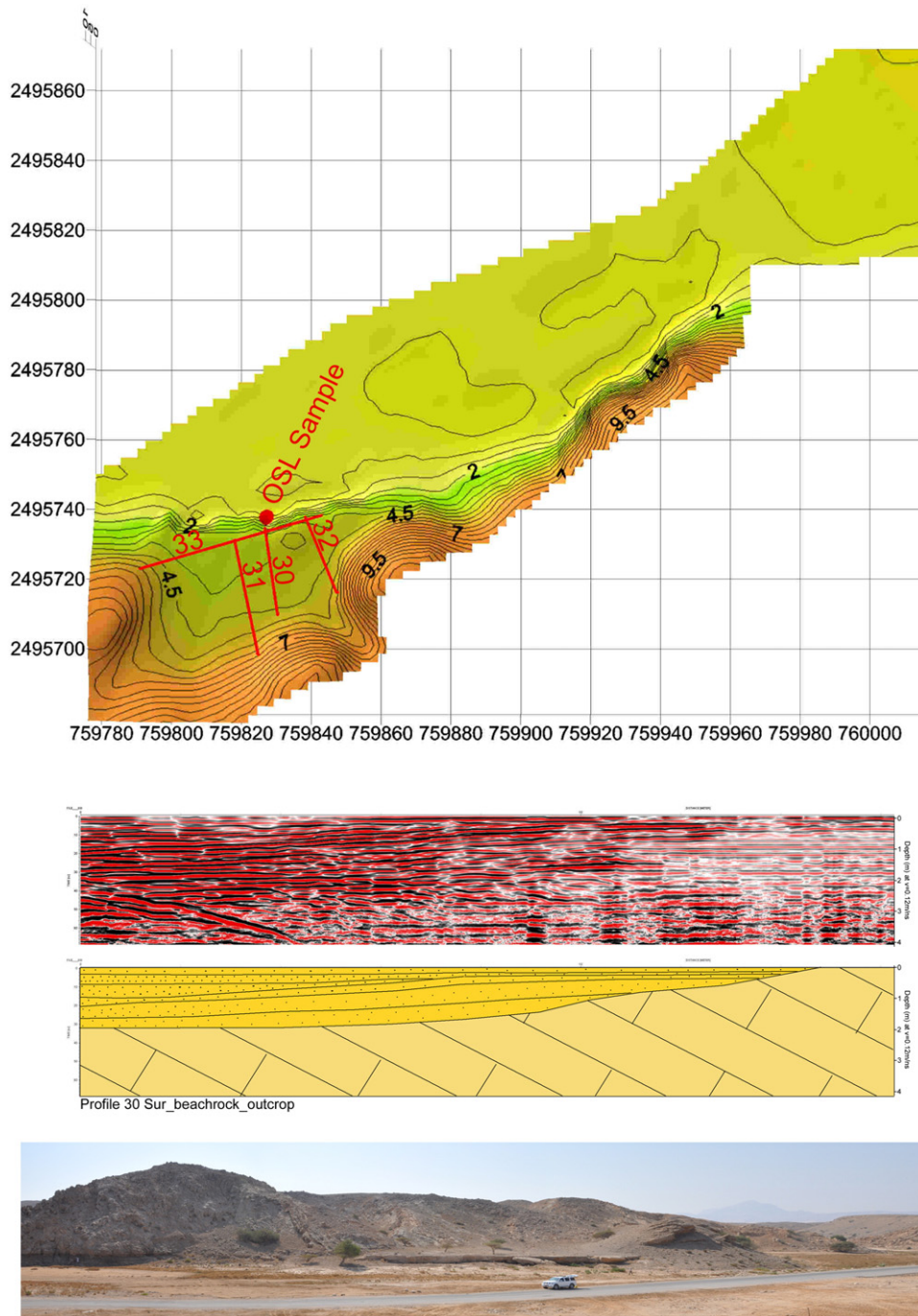
Fig. 5. GPR image illustrating the potential of the technique if beachrock is situated away from modern marine zone.

3.4. Dating

Radiocarbon and optically stimulated luminescence (OSL) are the two most suitable dating techniques for determining the age of a deposit. OSL relies on the exposure of quartz grains to daylight. During formation of the beachrock, the grains are sheltered from daylight and acquire a luminescence signal by exposure to environmental radioactivity. For radiocarbon dating, shells or cement can be used. While all the material (quartz, cement and shell) of a sample should deliver the same age due to the negligible time lag between sedimentation and cementation, the accuracy of an age depends on the a number of requirements specific to the technique. For the OSL technique it is the ability to reconstruct the change of dose rate during burial (Nathan and Mauz, 2008) and to detect the time-sensitive signal from quartz

(Aitken, 1998). For radiocarbon it is the ability to correct for isotope fractionation and reservoir effects, in particular when cement is used because its carbon isotopes originate from two solutions with two different isotopic compositions. As a result both the marine reservoir effect and the terrestrial hardwater effect must be considered, which might be difficult in practice without information from additional stable isotopes (e.g., strontium).

Thomas (2009) was the first to employ the OSL technique to accurately date beachrock deposits occurring on the coast of southeast India. An OSL data set is listed in Tables 2, 3 and 4. One of the samples listed (LV426) demonstrates the importance of dating: the morphological setting of the site (Fig. 7) suggests a deposit of Holocene age while the OSL age of the beachrock surface is around 80 ka suggesting that the RSL was situated at the modern level during MIS 5a.

Fig. 6. Thin section images of beachrock deposits (North Africa, Mediterranean Sea). A — moderately sorted oolitic grainstone with isopachous HMC rim (dull blue in CL) indicative for the lower intertidal zone. B — Well-sorted mixed bio-siliciclastic grainstone with syntaxial echinoderm overgrowth and circumgranular calcite, which is blue in CL with an outer band of violet colour. Isopachous fabric and fain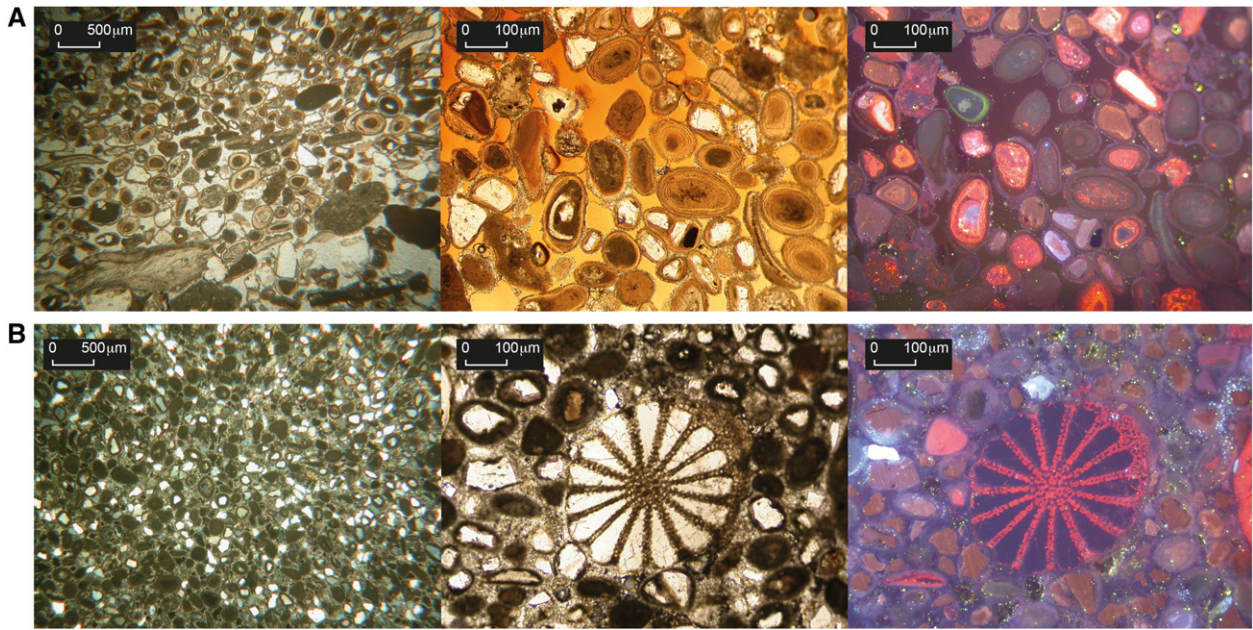t Mn as CL activator indicate precipitation from oxidising water under shallow marine conditions in the lower intertidal zone.

A comparison between ages obtained from radiocarbon and OSL dating techniques shows systematically lower OSL age values regardless of the calibration curve used for radiocarbon, the differences within ^{14}C or whether whole rock or shell was used (Bosman, 2012). Ages obtained from mollusc shells tend to agree better with quartz OSL ages (Bosman, 2012). As such, careful selection of the material used for radiocarbon dating can circumvent the effect of old carbon and diagenesis (e.g., Desruelles et al., 2009).

4. Establishing a sea-level index point

To qualify as a sea-level index point (SLIP), the sea-level indicator has to be characterised by (1) location, (2) age, (3) sampling elevation and (4) indicative meaning which is the known relationship between the indicator and the corresponding shoreline (van de Plassche, 1986; Shennan, 1986). This known relationship is described by the reference water level and the midpoint of the indicative range where the indicative range is the elevation range occupied by the sea-level indicator (Shennan, 1986; van de Plassche, 1986). The sea-level indicator with its known indicative range is converted into a SLIP once its age is known.

An undisturbed in situ beachrock is a sea-level indicator on the basis of its cement and its sediment texture and bedding structures. The clarity of its indicative meaning depends largely on the preservation of the original cement and the ability to link cement with other sedimentary information.

In the intertidal zone the metastable aragonite and HMC form as rim cements. This fabric linked with small-scale trough cross bedding is indicative of the lower intertidal zone. Its indicative range spans from mean low water level (MLW) to mean tidal level (MTL) and, using the midpoint of this zone as reference water level, the associated error is half the tidal amplitude ($a_1/2$, where a = tidal amplitude). When this fabric is linked with low angle seaward-dipping tabular cross bedding and keystone vugs, the indicative range spans from MTL to mean high water level (MHW) and the error term is $a_2/2$. In the absence of sediment bedding information, the indicative range associated with the intertidal cement fabrics ranges from the MLW to the MHW. The zone is called 'undifferentiated intertidal' and its error term is $a_1 + a_2$ which is the average tidal range.

Samples exhibiting sparitic cements infilling cavities, micrite forming meniscus between grains and internal sediments as geopedal infilling are characteristic of the vadose zone. The relationship of these

Table 2
Description of beachrock samples dated using the OSL technique. The model used to determine the equivalent dose (D_e) is listed in Table 4.

Sample code (LV)	Origin	Coordinates	D_e (median) $\pm \sigma$ (Gy)	D_e (model, Gy)	OSL age (ka, $\pm 1\sigma$)
249	E-Mediterranean (Levant)	32.14N 34.49E	1.20 ± 0.33	1.1 ± 0.1	2.3 ± 0.1
365	Levant	32.40N 34.56E	84 ± 2	85 ± 1	113 ± 5
404	Levant	32.49N 34.57E	0.51 ± 0.02	0.51 ± 0.02	1.01 ± 0.06
426	Iberia (Torre Vieja)	37.56N 00.42E	79 ± 4	73 ± 5	83 ± 6
493	Gulf of Gabès	33.64N 10.55E	3.37 ± 0.09	3.3 ± 0.1	4.3 ± 0.2
494	Gulf of Gabès	33.64N 10.56E	80 ± 3	82 ± 3	106 ± 4
565	E-Arabia (Oman)	22.30N 59.56E	50 ± 3	48 ± 3	80 ± 3

Table 3
Analytical data used for OSL age estimation. For details on age modelling of carbonate-rich sediments see Nathan and Mauz (2008).

Sample code (LV)	Grain size (µm)	Water content (%)	U (µg g^{-1})	Th (µg g^{-1})	K (wt.%)	D_{cosm} (Gy ka^{-1})	Carbonate (%)
249	180–250	8 ± 3	0.399 ± 0.018	0.626 ± 0.063	0.169 ± 0.010	0.212 ± 0.010	71 ± 4
365	150–200	5 ± 3	1.353 ± 0.036	0.763 ± 0.058	0.227 ± 0.010	0.153 ± 0.008	60 ± 3
404	200–250	5 ± 3	0.247 ± 0.012	0.288 ± 0.069	0.194 ± 0.010	0.21 ± 0.01	65 ± 4
426	200–250	5 ± 2	1.156 ± 0.032	1.785 ± 0.069	0.474 ± 0.014	0.21 ± 0.01	75 ± 4
493	200–300	5 ± 2	1.440 ± 0.035	0.765 ± 0.039	0.072 ± 0.006	0.21 ± 0.01	87 ± 5
494	90–150	6 ± 2	1.732 ± 0.045	0.679 ± 0.058	0.201 ± 0.010	0.098 ± 0.004	69 ± 4
565	200–300	5 ± 2	1.708 ± 0.045	0.796 ± 0.085	0.122 ± 0.009	0.172 ± 0.009	90 ± 3

Table 4
Analytical and statistical data used to estimate the equivalent dose (D_e). For details on statistics see Galbraith and Roberts (2012).

Sample code (LV)	Aliquot# (accepted/measured)	Aliquot size (mm)	Rejection			Descriptive statistics				Statistical age model
			$D_0 < 53$ Gy	RR1/2	Dim/fit	σ (%)	c	s	k	
249	33/72	3	n/a	18	21	43 ± 5	−0.85	0.33	1.07	CAM
365	22/72	3	31	1	18	28 ± 5	−1.06	−1.1	−0.25	CAM
404	42/96	5	n/a	35	19	24 ± 3	0.86	0.25	2.79	Median
426	22/24	3	–	–	2	39 ± 6	−0.87	0.39	0.89	CAM
493	168/38	3	n/a	57	73	15 ± 2	−0.37	0.16	0.38	CAM
494	31/96	3	22	18	25	17 ± 3	0.94	0.189	1.61	CAM
565	23/111	3	57	24	7	24 ± 4	−0.13	0.26	−0.07	CAM

samples with a former tidal level is the upper intertidal zone and the spray zone. The elevation of this zone depends on wave exposure and the local geomorphology (Leeuw et al., 2000). For error calculation we include the spray zone due to its potential contribution to the cementation so that the error term is $(a_2/2) + s$, where s is the elevation of the spray zone. Low angle seaward-dipping tabular cross bedding occurring together with keystone vugs provide an upper intertidal indicative range (but no example of this assemblage was found in literature). In the absence of sediment bedding information, samples exhibiting these types of cement fabric provide a terrestrial limiting point (i.e., MTL is situated below this point). Likewise, samples showing LMC equant spar crystals (typically consisting of equigranular, anhedral to subhedral crystals) formed near or above the high tide and represent a terrestrial limiting point.

Where only sediment bedding information is available, the indicative meaning is less precise. Small-scale trough cross-bedding is generally

evidence of the lower intertidal environment (Strasser and Davaud, 1986; Bezerra et al., 2003; Caldas et al., 2006) and without cement information, such samples represent a marine limiting point (i.e., MTL is above this point). Likewise, low angle seaward dipping tabular cross bedding indicates upper intertidal to supratidal formation (Bezerra et al., 2003) and without cement information, these samples should be used as a terrestrial limiting point (i.e., MTL is below this point). However, in the presence of keystone vugs, an indicative range from MTL to MHW with an error term of $a_2/2$ can be ascribed (Dunham, 1970; Strasser and Davaud, 1986). Notwithstanding this evidence, marine cements should be present to ascribe the sample to the upper intertidal zone (Desruelles et al., 2009). A summary of indicative meaning and error terms is provided in Table 5 and Fig. 8.

The total uncertainty of this vertical shoreline reconstruction is quantified from levelling, indicative range (as described above) and tidal range, applying the square root rule (i.e., $\sqrt{a^2 + b^2 + c^2}$, where a,

Fig. 7. The coast at Torre Vieja (37°N, 00°E) and its beachrock deposit. The morphological setting suggests a Holocene age of the deposit while its OSL age (83 ± 6 ka) suggests a RSL level similar to today during MIS 5a. For scale see person (ca 1.60 m).

Table 5
Indicative meanings of beachrock with respect to the sea-level index point (SLIP) and limiting point. Reference water level for all SLIPS is the midpoint between the relevant water levels. Mean tidal level (MTL) is the mean sea level (0 m); the vertical distance between mean high water (MHW) and mean low water (MLW) constitutes the tidal range which ideally oscillates symmetrically around the mean; tidal amplitude is half of the tidal range; a_1 = tidal amplitude between MTL and MLW; a_2 = tidal amplitude between MTL and MHW; d = maximum water depth of beachrock formation zone (typically upper shoreface); s = elevation of the spray zone.

Sample evidence	SLIP	Indicative meaning	±
Irregularly distributed needles or isopachous fibres of aragonite or isopachous rims (bladed or fibrous) and micritic HMC cement and small-scaled trough cross stratification	Lower intertidal	MTL to MLW	$a_1 / 2$
Irregularly distributed needles or isopachous fibres of aragonitic cement or isopachous rims (bladed or fibrous) and micritic HMC cement or HMC cement in stalactitic position and meniscus between grains and low angle seaward dipping tabular cross bedding with the presence of keystone vugs	Upper intertidal	MHW to MTL	$a_2 / 2$
Irregularly distributed needles or isopachous fibres of aragonitic cement or isopachous rims (bladed or fibrous) and micritic HMC cement without bedding architecture information	Intertidal, undifferentiated	MHW to MLW	$a_1 + a_2$
Small-scale trough cross stratification without cement fabric and chemistry information	Marine limiting	Below MTL	$a_1 + d$
HMC cement in stalactitic position and meniscus between grains and internal sediments	Terrestrial limiting	Above MTL	$a_2 + s$
Low angle seaward dipping tabular cross bedding without keystone vugs and cement fabric and chemistry information			
Equant or subequant spar of LMC cement			

b, c are the independent error terms of levelling, tidal range and indicative meaning respectively).

We assume negligible beachrock formation in the zone of the highest tide and use the spring/neap tide range as an error of tidal range. Other potential errors such as changes in the water table and sediment compaction are regarded as negligible due to the instantaneous cementation of the sediment.

5. Relative sea-level reconstruction using beachrock

We outline previous work where beachrock was used for RSL reconstruction. The most comprehensive studies are described in the text and other relevant studies are listed in Table 6. The compilation focuses on sediment characteristics and techniques used to determine a SLIP and builds on the review of Vousdoukas et al. (2007) where formation and cementation processes as well as criteria for identification are described. The map in Fig. 9 displays the spatial distribution of beachrock-based RSL reconstructions listed in Table 6.

Most authors used the cement type to infer the position of the shoreline with uncertainties between 0.5 m and 1.5 m (Table 6). The standard setting for this approach was Strasser et al. (1989) who used data from field surveying, petrography, microprobe and SEM analyses to infer timing of cementation and migration of shoreline.

Desruelles et al. (2009) built on the example of Strasser et al. (1989) and determined the indicative meaning through SEM, petrographic and cathodoluminescence analyses and used keystone vugs to determine the position of the sea level with a precision of ±0.25–0.50 cm. The radiocarbon age of the deposits was obtained using the cement and the ages seem to confirm that the hand-picked samples were not contaminated by external carbonate. Studying details of the cement, Vacchi et al.

(2012a) found primary marine phreatic cement, typical for the intertidal zone, followed by meteoric cement and bioclast dissolution. These findings allowed the authors to correlate the beachrock with other RSL indicators in order to reconstruct palaeo-shorelines in distinct tectonic domains.

Some authors combined evidence from cement, sediment bedding and local features to reconstruct the shoreline. Michelli (2008) and Stattegger et al. (2013) linked saltmarsh, mangrove and beachrock deposits to reconstruct the RSL. The relationship of each sample with the contemporary tidal levels was assessed through sediment bedding and cement analysis. Radiocarbon dating was performed on well preserved marine shells and coral fragments in beachrock samples. Ramsay (1995) established a RSL curve based entirely on beachrock observational data. The indicative meaning was deduced from the present-day beach where beachrock forms at 10–20 cm above mean sea level and from the presence of aragonitic rim cements. These were interpreted as indicating shoreline position with an uncertainty of 0.5 m (Ramsay, 1995). The modern beachrock deposits were later ascribed to the intertidal environment due to their position at mean low tide level and the cementation by micritic, aragonitic and iron oxide infilled voids (Cawthra and Uken, 2012). Cawthra et al. (2012) revisited these deposits and found micritic coatings followed by isopachous prismatic crystal rims and equant calcite spars in pores often capped by cryptocrystalline coatings. On the basis of this two-step cementation history, alongside trough cross-bedded and often heavy mineral lined foresets, the depositional environment was considered intertidal, analogous with the low tide trough of contemporary beaches. Bosman (2012) confirmed the intertidal environment and determined a 2 m uncertainty based on the position of the modern beachrock and the tidal range.
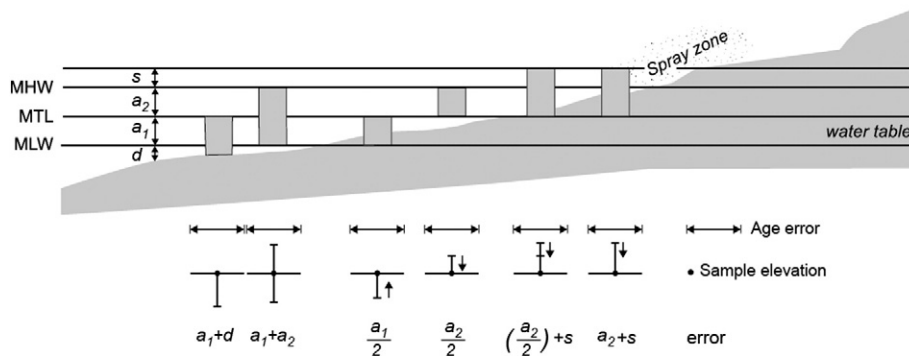
Fig. 8. Illustration of indicative range of beachrock and associated error. The indicative range spans from upper shoreface to spray zone encompassing the range from mean low water level (MLW) to mean high water level (MHL). The midpoint of each zone is the reference water level. The minimum vertical error is half the tidal amplitude ($a / 2$) and the maximum error is the tidal range ($a_1 + a_2$). Tidal amplitude is half of the tidal range; a_1 = tidal amplitude between MTL and MLW; a_2 = tidal amplitude between MTL and MHW; d = maximum water depth of beachrock formation zone (typically upper shoreface); s = elevation of the spray zone.

Table 6

Beachrock characteristics and dating techniques used in studies. Listed are attributes used to establish the indicative meaning. Columns in italic indicate new interpretation inferred from our approach. Error of time is combined systematic and random uncertainty of respective dating technique (not listed). For details of indicative meaning and uncertainty see Table 5. Ar = aragonite; LMC = low magnesian calcite; HMC = high magnesian calcite.

Region	Site	Reference	Dating (material; technique)	Sediment bedding and architecture	Primary chemistry and mineralogy	Primary fabric	Other observations	Markers used for indicative meaning	Authors' indicative meaning and uncertainty	New indicative meaning	Uncertainty
South Africa	False bay (34°S)	Siesser (1974)	Bulk carbonate; ^{14}C	Not provided	LMC; Ar	Isopachous micritic rim	Extensive solution pits and vertical channels in the rock	Modern analogue; fossil assemblage; cement	Upper intertidal	(MHW − MTL) / 2	Tidal amplitude (MTL to MHW)
Mozambique	Vilan-culo (22°S)	Siesser (1974)	Bulk carbonate; ^{14}C	Not provided	Ar	Isopachous fibrous needles	Intertidal fossil assemblage	Modern analogue; fossil assemblage; cement	Intertidal	(MHW − MLW) / 2	Tidal range
Brazil	Macau (1°S)	Bezerra et al. (2003)	Articulated shell; ^{14}C	Trough-cross bedding	Not provided	Not provided	Not provided	Sediment bedding	Lower foreshore to upper shoreface, ±1 m	MTL	Undefined
Brazil	Macau (1°S)	Bezerra et al. (2003)	Articulated shell; ^{14}C	Seaward dipping swash-cross beds	Not provided	Not provided	Not provided	Sediment architecture	Mid to lower foreshore, ±1 m	MTL	Undefined
Greece	Mykonos (37°N)	Desruelles et al. (2009)	Bulk carbonate; ^{14}C	Not provided	HMC	Isopachous small bladed rim	Not provided	Cement	Intertidal, ±0.5 m	(MHW − MLW) / 2	Tidal range
Greece	Delos (37°N)	Desruelles et al. (2009)	Bulk carbonate; ^{14}C	Not provided	HMC	Isopachous small bladed rim	Not provided	Cement	Intertidal, ±0.5 m	(MHW − MLW) / 2	Tidal range
Greece	Delos (37°N)	Desruelles et al. (2009)	Bulk carbonate; ^{14}C	Not provided	HMC	Internal sediments	Not provided	Cement	Intertidal, ±0.5 m	(MHW − MLW) / 2	Tidal range
Greece	Rhenia (37°N)	Desruelles et al. (2009)	Bulk carbonate; ^{14}C	Not provided	HMC	Isopachous small bladed rim	Not provided	Cement	Intertidal, ±0.5 m	(MHW − MLW) / 2	Tidal range
Turkey	Kemer (36°N)	Desruelles et al. (2009)	Cement; ^{14}C	Not provided	HMC	Internal sediments	Not provided	Cement	Intertidal, ±0.5 m	(MHW − MLW) / 2	Tidal range
Turkey	Kemer (36°N)	Desruelles et al. (2009)	Cement; ^{14}C	Not provided	Ar	Fibrous needles	Not provided	Cement	Intertidal, ±0.5 m	(MHW − MLW) / 2	Tidal range
Turkey	Gozculer (36°N)	Desruelles et al. (2009)	Cement; ^{14}C	Not provided	HMC	Isopachous fibrous rim	Not provided	Cement	Intertidal, ±0.5 m	(MHW − MLW) / 2	Tidal range
Egypt	Alexandria (31°N)	El Sayed (1988)	No dating	Not provided	HMC	Isopachous micritic rim	Not provided	Not provided	Not provided	(MHW − MLW) / 2	Tidal range
Egypt	Safaga (34°N)	Holail and Rashed (1992)	No dating	Not provided	HMC, Ar	Isopachous micritic and fibrous rim	Not provided	Not provided	Not provided	(MHW − MLW) / 2	Tidal range
Egypt	El Daba (31°N)	Holail and Rashed (1992)	No dating	Not provided	HMC, Ar	Isopachous micritic and fibrous rim	Not provided	Not provided	Not provided	(MHW − MLW) / 2	Tidal range
Togo	Lomè (6°N)	Amieux et al. (1989)	Mollusc shell; ^{14}C	Cross bedding	HMC, Ar, LMC	Isopachous micritic and fibrous rim	Not provided	Not provided	Not provided	MLW to supratidal	Tidal range
Belize	Cay (16°N)	Gischler and Lomando (1997)	Bulk carbonate; ^{14}C	Not provided	Ar; HMC	Isopachous micritic and fibrous rim	Not provided	Cement	Marine-phreatic zone	(MTL + MLW) / 2	Tidal amplitude (MHW to MTL)
Vietnam	Cà Nà (10°N)	Michelli (2008), Stattegger et al. (2013)	Coral and Bivalve; ^{14}C	Cross bedding	HMC, Ar	Isopachous micritic and fibrous rim	Not provided	Sediment architecture; cement	Intertidal, ±1.15 m	(MHW − MLW) / 2	Tidal range
Italy	Sardinia (40°N)	Lambeck et al. (2004)	Bulk carbonate; ^{14}C	Cross bedding	HMC	Isopachous fibrous rim	Not provided	Cement	Palaeo-shoreline, +1 m, −5 m	MTL	Undefined
Turkey	Thracia Black Sea (41°N)	Erginal et al. (2013)	Bulk carbonate; ^{14}C	Not provided	LMC	Micritic	Not provided	Cement	Upper intertidal	(MHW − MTL) / 2	Tidal amplitude (MTL to MHW)
Brazil	Cabelo (12°S)	Caldas et al. (2006)	Bivalve; ^{14}C						Swash-cross-bedding	Not provided	Not provided
Not provided	Modern analogue; sediment architecture	Foreshore, ±1.4	MTL	Undefined							

Saudi Arabia	Al-Shoaiba (20°N)	Ghandour et al. (2014)	No dating	Low-angle cross-bedding	Ar, HMC	Isopachous micritic and fibrous rim	Not provided	Cement	Marine-phreatic	(MTL + MLW) / 2	Tidal amplitude (MTL to MLW)
Spain	Galicia (9°N)	Rey et al. (2004)	No dating	Not provided	LMC	Isopachous fibrous rim	Meniscus	Not provided	Supratidal	MTL	Undefined
Spain	La Palma (28°N)	Calvet et al. (2003)	Cement; ^{14}C	Not provided	Ar, HMC	Isopachous fibrous needle, isopachous spar rim, isopachous micritic rim	Meniscus	Cement	Intertidal to upper shoreface	MTL	Tidal range
USA	Florida (27°N)	Spurgeon et al. (2003)	Bulk carbonate and cement; ^{14}C	Swash cross bedding and landward-dipping beds	LMC	Blocky spar rim; isopachous bladed spar rim	Not provided	Sediment architecture and cement	Supratidal	MTL	Undefined
India	Maharastra (18°)	Badve et al. (1997)	Gastropod; ^{14}C	Not provided	Ar	Isopachous fibrous rim	Fossil assemblage	cement	Lower intertidal	(MTL + MLW) / 2	Tidal amplitude (MLW to MTL)
Turkey	Parion (40°N)	Erginal (2012)	Bulk carbonate; ^{14}C	Not provided	HMC	Micritic	Meniscus, dissolution pits of meteoric water	Cement	Intertidal to supratidal	MTL	Undefined
Israel	Tel Haratz (31°)	Bakler et al. (1985)	Shell; ^{14}C	Low angle cross bedding	Ar, LMC	Isopachous fibrous needle rim, blocky	Not provided	Sediment architecture and cement	Intertidal to supratidal	(MHW − MTL) / 2	Tidal amplitude (MHW to MTL)
South Africa	Sodwana bay (27°S)	Ramsay (1995), Ramsay and Cooper (2002)	U-series (^{234}U/^{230}Th)	Basal unit of a beachrock--aeolianite complex	Not provided	Isopachous fibrous rim, blocky equant	Not provided	Sediment architecture	Palaeo-sea level, ± 1.5	MTL	Undefined
Greece	Kalamaki,Crete (35°N)	Neumeier (1998)	Bulk carbonate and bioclasts; ^{14}C	Not provided	HMC	Micritic, isopachous bladed spar rim		Cement	Intertidal	(MHW − MLW) / 2	Tidal range
French Polynesia	Taraire (17°S)	Neumeier (1998)	Bulk carbonate; ^{14}C	Not provided	Ar	Isopachous fibrous needle rim		Cement	Intertidal	(MHW − MLW) / 2	Tidal range
Egypt	Ras Garib (28°N)	Neumeier (1998)	Cement; ^{14}C	Not provided	Ar	Isopachous fibrous needle rim,	Not provided	Cement	Intertidal	(MHW − MLW)/2	Tidal range
Egypt	El Baida (25°N)	Neumeier (1998)	Cement; ^{14}C	Not provided	Ar	Isopachous fibrous needle rim,	Not provided	Cement	Intertidal	(MHW − MLW) / 2	Tidal range
Saudi Arabia	Aqaba gulf (28°N)	Al-Ramadan (2013)	Bulk carbonate; ^{14}C	Low angle seaward dipping cross beds	Ar; HMC	Isopachous fibrous needle, micritic	Not provided	Cement	Intertidal	(MHW − MLW) / 2	Tidal range
Saudi Arabia	Arabic gulf (25°N)	Al-Ramadan (2013)	Bulk carbonate; ^{14}C	Low angle seaward dipping cross beds	Ar; HMC	Isopachous fibrous needle, micritic	Not provided	Cement	Intertidal zone	(MHW − MLW) / 2	Tidal range
Australia	Shark bay (25°S)	Neumeier (1998)	Bulk carbonate; ^{14}C	Not provided	Ar	Isopachous micritic, isopachous fibrous needle	Not provided	Cement	Intertidal	(MHW − MLW) / 2	Tidal range
Greece	Lesvos (39°N)	Vacchi et al. (2012a)	Bioclasts; ^{14}C	Not provided	HMC	Isopachous Micritic, isopachous fibrous	Not provided	Cement	Palaeo-sea level, ± 0.5	(MHW − MLW) / 2	Tidal range
Tunisia	Bahiret el Biban (33°N)	Strasser et al. (1989)	Bulk carbonate; ^{14}C	Seaward dipping beds	Ar; HMC	Isopachous fibrous needle; isopachous spar	Keystone vugs	Sediment architecture and cement	Palaeo shoreline	(MHW − MLW) / 2	Tidal range
Spain	Bilbao (43°N)	Arrieta et al. (2011)	Modern fragments cemented in beachrock	Parallel laminated seaward dipping beds	Ar; HMC	Isopachous fibrous needle; micritic	Conglomeratic beds with imbricated clasts	Sediment architecture and cement	Shoreface to foreshore	(MTL + MLW) / 2	Tidal amplitude (MLW to MTL)
China	Haishan Island (23°N)	Fuzhi and Youshen (1988), Shen et al. (2013)	Shell; ^{14}C	Low angle seaward dipping cross beds	Ar, LMC	Micritic, isopachous fibrous needle, spar	Fossil assemblage	Sediment architecture, fossils and cement	Semi-enclosed lagoon; intertidal to supratidal	(MTL − MLW) / 2	Tidal amplitude (MHW to MTL)
Bahamas	Bimini (25°N)	Strasser and Davaud	No dating	Seaward dipping tabular cross	Ar	Isopachous fibrous needle	Keystone vugs	Sediment architecture and	Upper intertidal	(MTL − MLW) / 2	Tidal amplitude (MHW to MTL)

Table 6 (*continued*)

Region	Site	Reference	Dating (material; technique)	Sediment bedding and architecture	Primary chemistry and mineralogy	Primary fabric	Other observations	Markers used for indicative meaning	Authors' indicative meaning and uncertainty	*New indicative meaning*	*Uncertainty*
		(1986)		beds with keystone vugs				cement			
Bahamas	Joulter Cays (25°N)	Strasser and Davaud (1986)	No dating	Seaward dipping tabular cross beds	Ar	Isopachous fibrous needle	Keystone vugs	Sediment architecture and cement	Upper intertidal	*(MTL − MLW) / 2*	*Tidal amplitude (MHW to MTL)*
USA	Maui (21°N)	Meyers (1987)	No dating	Not provided	HMC	Isopachous rim	Meniscus	Cement	Marine vadose zone of the beach	*(MTL − MLW) / 2*	*Tidal amplitude (MHW to MTL)*
Gran Cayman	Car (19°N)	Moore (1973)	No dating	Not provided	Ar, HMC	Isopachous fibrous, micritic or bladed rim	Not provided	Cement	Intertidal	*(MHW − MLW) / 2*	*Tidal range*
Bahamas	San Salvador (24°N)	Kindler and Bain (1993)	Bulk carbonate; ^{14}C	Low angle seaward dipping planar lamination	Ar; LMC	Isopachous fibrous needle rim, micritic	Meniscus, keystone vugs	Stratification and cement	Intertidal to supratidal	*MTL*	*Undefined*

Fig. 9. Location of beachrock deposits used for RSL reconstruction. See Table 3 for references.

Bezerra et al. (1998) attributed medium to coarse sandstone that was deposited in seaward dipping cross-stratified beds with increasing grain size seawards, to the middle to lower foreshore with a RSL precision of ±1 m. With medium to fine sandstone the upper shoreface part of the deposit was identified and the corresponding position of the shoreline was estimated with an error of ±0.5 m. Vieira et al. (2007) refined this approach by mapping out lithofacies with distinct characteristics relevant for the position of the corresponding shoreline.

A few authors have used the associated coastal fauna. Yaltirak et al. (2002) identified the beachrock deposits situated in various altitudes above modern sea level through the presence of the fauna *Balanus*, *Alvania lacteal* and *Truncatella subcylindrica* and deduced the indicative meaning through comparison with the modern analogue. In this study U-series dating on shells was employed resulting in consistent MIS 5e and MIS 7 ages but also with some age reversals and unexplained age differences.

Beachrock deposits occur not only on modern coasts above or a few metres below water level, but also on submerged continental shelves where access is more challenging. Bosman (2012) used high-resolution geophysical profiling and sampling to establish a geological map that included 3 distinct beachrock ridges situated in around 25 m water depth. Using a similar method, Locker et al. (1996) mapped 4 distinct ridges partly composed of beachrock, which occur between 120 m and 60 m water depth. Two of these ridges may have recorded the meltwater pulse 1A. This and subsequent studies (Jarrett et al., 2005; Gardner et al., 2007; Green et al., 2014) show also, that laterally continuous shoreline deposits can form at the edge of the shelf in places where the steepness of the slope is reduced to around 0.02 m/m.

6. The beachrock tool: an example

We highlight an example where beachrock data collected from an outcrop was used to infer the local RSL history.

In the Gulf of Gabès (south Tunisia) RSL observational data were generated through conventional field mapping, logging and elevation measurements using differential GPS. Present-day mean low and high tide shorelines were mapped from morphological evidence. Mean tidal range and mean astronomical tidal range were obtained from tide gauge data (station Ganouch; Sammari et al., 2006) and were taken into account to estimate the indicative range and its error. Texture, composition and matrix properties of sediment samples were identified from thin sections, and the carbonate mineralogy was studied using cathodoluminescence. OSL dating of quartz and radiocarbon dating of mollusc shells (Morhange and Pirazzoli, 2005) were used for age estimation.

In the coastal cross-section (Fig. 10) the succession of two beachrock deposits was identified. One is composed of planar beds of moderately sorted oolitic grainstone with isopachous HMC rim and scalenohedral dog tooth cement (Fig. 6A). Its age is around 6 ka and its elevation is 1.1 ± 0.22 m. Onlapping this is a well-sorted mixed bio-siliciclastic
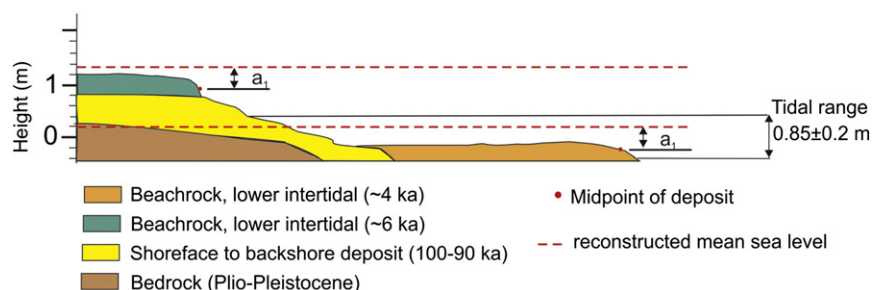

Fig. 10. Cross section at El Grine illustrating two Holocene beachrock deposits with their indicative meaning and associated uncertainty.

grainstone with circumgranular HMC, which is blue in CL with an outer band of violet colour (Fig. 6B). Its age is around 4 ka and its elevation is 0.0 ± 0.23 m.

Oolitic grainstone with isopachous HMC rim formed in the lower intertidal and was subsequently subjected to the upper intertidal. Assuming the geometry of this tectonically stable coast has not changed during the Holocene and the mean tidal range was therefore constant at 0.85 ± 0.2 m, the indicative meaning of both SLIPs is -0.4 ± 0.2 m. With the reference water level being the midpoint of the intertidal deposit, the shoreline of the mid Holocene deposit was then reconstructed to 1.4 ± 0.4 m and the one of the onlapping deposit to 0.2 ± 0.4 m. The error is derived from the square root of the sum of error values.

7. Discussion

Beachrock forms in the mixing zone between the upper shoreface and the beach where sand-sized sediment is available and the morphology is suitably flat. The criteria to identify the sub-environment are based on cement and bedding structure where the cement should be described in terms of chemistry, crystal form and fabric. Integration of these criteria allows establishing indicative meaning and vertical error and resolves doubts (cf., Kelletat, 2006).

7.1. Shelf morphology and RSL change

While beachrock formation is relatively independent on coastal morphology, the preservation of the deposits is less likely to occur below the shelf edge where a steep gradient creates reflective beach morphologies. The use of beachrock for sea-level reconstruction may therefore be restricted to the interval when the sea level is situated on the shelf, and, in many cases, on the inner shelf. It is unlikely that beachrock forms a large-scale feature on the shelf when RSL rise exceeds ~12 mm/a because the shoreface (main source of sediment for the intertidal zone on subtropical coasts) is reworked at a rate that precludes preservation of the adjacent beach. Beachrock can form in patches when RSL rise is <12 mm/a because sufficient sediment would be available in places and, after 20 years of lithification time, the RSL would still be within the same intertidal zone. Beachrock forms on a larger spatial scale with RSL rise < 5 mm/a (Vousdoukas et al., 2007). As Quaternary RSL falls on average with a slower rate than it rises, it can be hypothesised that most of the beachrock fields represent a falling RSL. Either way, beachrock formation does not require a RSL stillstand; more important is a continuous and almost constant carbonate accumulation rate when sea-surface temperature (SST) falls during cool climate periods. For example, in the oligotrophic western (sub-)tropical Atlantic where beachrock fields are frequent, carbonate accumulation was nearly constant during the last glacial/interglacial transition (Arz et al., 1998) so that the carbonate factory did not slow down during cool climate periods. But this might not have been the same elsewhere and continuous beachrock formation in cooling coastal waters remains to be shown by data from the currently inundated shelves.

7.2. Cement

There has been a considerable amount of confusion about the interplay between cementation processes and geomorphological position leading some authors to express misgivings on the reliability of beachrock as a sea-level indicator (e.g., Kelletat, 2006) with subsequent discussion (Knight, 2007). The comprehensive review of Vousdoukas et al. (2007) has removed these doubts and clarified that the cement is crucial for identifying the spatial relationship between coastline and beachrock formation zone. This key element in RSL reconstruction can be masked by multiple phases of rim cement formation, dissolution or other geochemical reorganisation where the pathway of diagenesis is dependent on the original mineralogy of the sediment undergoing

alteration and on the chemistry of the overlying bed. While staining and cathodoluminescence are excellent tools to establish cement zoning, this analysis is probably the most challenging part of the SLIP investigation and age determination if cement is used. The typical reorganisation with rising RSL is micritisation of biotic and abiotic calcite and aragonite, dolomitisation in the sulphate reduction zone and with falling sea level it is dissolution and recrystallisation of aragonite to calcite and HMC to LMC. In case of complete diagenesis the depositional origin may be hard to identify and the cement should not be used for age determination.

The cementation rate is most rapid in the landward side of the beachrock formation zone where large carbonate crystals fill pore space and bind components within the space of years to decades. Thus, before burial the sediment is already lithified and is likely not subject to compaction that would be significant enough to impact on the vertical precision of the SLIP.

7.3. Chronology

Suitable techniques to determine the age of a beachrock sample are OSL and radiocarbon. U-series, in particular when using mollusc shells is unsuitable (Kaufman et al., 1971; Mauz and Antonioli, 2009) due to the significant geochemical alterations and associated uranium isotope ratio and profile across the shell. There are many examples that show that even corals, in particular non-tropical species, suffer from diagenetic alteration impacting on the accuracy of an age derived from U-series technique (e.g., Leeder et al., 2003; Amorosi et al., 2014).

7.4. Precision

Hopley (1986) expressed concerns with regard to height relationships because the upper limit of beachrock cementation would not be well defined. Indeed, given the potential impact of sea-water spray on cementation, the limits of the former intertidal zone may be difficult to determine on the basis of the cement alone; information on the tidal regime is also required. Ideally, lateral facies relationships based on a transect across and beyond the beachrock formation zone is also established.

Beachrock is an intertidal deposit. The vertical error of the RSL reconstruction is therefore a result of the 3 error terms derived from levelling, indicative range and tidal range. The precision can be raised up to half of the tidal amplitude by combining cement with facies analysis. Most beachrock deposits occur on microtidal coasts with an average thickness of 2 m (e.g., Cooper, 1991); thus, the vertical errors typically fall between 2 m and 0.1 m, where the larger error can be avoided if cement rather than thickness or lateral extend of the deposit (e.g., Lambeck et al., 2004) is used. While these error bars are comparable to RSL reconstructions derived from saltmarshes (e.g., Barlow et al., 2013; Mills et al., 2013), they are bigger than those derived from microbial mats (Livsey and Simms, 2013). They benefit, however, from the lack of additional error terms that are hard to quantify (e.g., compaction). The beachrock-based reconstruction can be an order of magnitude more precise than that obtained from corals due to the essentially unknown fluctuations of reef growth even under relatively constant environmental conditions (Perry and Smithers, 2011). Notwithstanding this, any direction of shoreline migration is hard to infer from beachrock. The deposit is usually a singularity and lacks backstepping or prograding architecture and related bounding surfaces.

8. Conclusions

We have shown that a beachrock deposit is a reliable RSL marker. It can be used to increase the number of RSL observations in the far-field and it can be used to test coral-based RSL records. The error of the beachrock-based RSL reconstruction is comparable to other RSL markers with the advantage that there are no additional, hard to quantify error terms.

A beachrock deposit is not continuous, but a point in time and space. Its zone of formation is limited to coasts with low sedimentation rate, relatively flat morphology and warm SST. How a drop in SST impacts on the continuity of formation at any particular location remains to be shown by investigating currently inundated shelves in the far-field.

References

Aitken, M., 1998. An Introduction to Optical Dating. Oxford Science Publications (289 pp.).

Alexandersson, T., 1985. Carbonate cementation in recent Coralline algal constructions. In: Toomey, D.F., Nitecki, M.H. (Eds.), Paleoalgology: Contemporary Research and Applications. Springer Verlag, Berlin Heidelberg, pp. 261–269.

Al-Ramadan, K., 2013. Diagenesis of Holocene beachrocks: a comparative study between the Arabian Gulf and the Gulf of Aqaba, Saudi Arabia. Arab. J. Geosci. http://dx.doi.org/10.1007/s12517-013-1127-7.

Amieux, P., Bernier, P., Dalongeville, R., Medwecki, V., 1989. Cathodoluminescence of carbonate-cemented Holocene beachrock from Togo coastline (West Africa): an approach to early diagenesis. Sediment. Geol. 65, 261–272.

Amorosi, F., Antonioli, F., Bertini, A., Marabini, S., Mastronuzzi, G., Montagna, P., Negri, A., Rossi, V., Scarpone, D., Taviani, M., Angeletti, L., Piva, A., Vai, G.B., 2014. The Middle–Upper Pleistocene Fronte Section (Taranto, Italy): an exceptionally preserved marine record of the Last Interglacial. Glob. Planet. Chang. 119, 23–38.

Antonioli, F., Anzidei, M., Lambeck, K., Auriemma, R., Gaddi, D., Furlani, S., Orrù, P., Solinas, E., Gaspari, S., Karinija, S., Kovacic, V., Surace, L., 2007. Sea-level change during the Holocene in Sardinia and in the northeastern Adriatic (central Mediterranean Sea) from archaeological and geomorphological data. Quat. Sci. Rev. 26, 2463–2486.

Arrieta, N., Goienaga, N., Martinez-Arkarazo, I., Murelaga, X., Baceta, J.I., Sarmiento, A., Madariaga, J.M., 2011. Beachrock formation in temperate coastlines: examples in sand-gravel beaches adjacent to the Nerbioi-Ibaizabal Estuary (Bilbao, Bay of Biscay, North of Spain). Spectrochim. Acta A Mol. Biomol. Spectrosc. 80 (1), 55–65.

Arz, H.W., Paetzold, J., Wefer, G., 1998. Correlated millennial-scale changes in surface hydrography and terrigenous sediment yield inferred from last-glacial marine deposits off northeastern Brazil. Quat. Res. 50, 157–166.

Badve, R.M., Rajshekhar, C., Kumaran, K.P.N., Kamble, C.V., 1997. On the age and fauna of beachrock of Kegaon Coast, Uran, Maharashtra. Curr. Sci. 72 (3), 168.

Bakler, N., Neev, D., Magaritz, M., 1985. Late Holocene tectonic movements at Tel Haraz, southern coast of Israel. Earth Planet. Sci. Lett. 75 (2), 223–230.

Barlow, N., Shennan, I., Long, A.J., Gehrels, W.R., Saher, M.H., Woodroffe, S.A., Hillier, C., 2013. Salt marshes as late Holocene tide gauges. Glob. Planet. Chang. 106, 90–110.

Bezerra, F.H.R., Lima-Filho, F.P., Amaral, R.F., Caldas, L.H.O., Costa-Neto, L.X., 1998. Holocene coastal tectonics in coastal Brazil. In: Steward, J., Vita-Finzi, C. (Eds.), Coastal Tectonics. Geological Society, London, Special Publications 146, pp. 279–293.

Bezerra, F.H.R., Barreto, A.M.F., Suguio, K., 2003. Holocene sea-level history on the Rio Grande do Norte State coast, Brazil. Mar. Geol. 196, 73–89.

Bosman, C., 2012. The marine geology of the Aliwal Shoal, Scottburgh, South Africa. (PhD thesis), University of KwaZulu-Natal, Durban (581 pp.).

Bristow, C.S., Jol, H.M., 2003. An introduction to ground penetrating radar (GPR) in sediments. Geol. Soc. Lond. Spec. Publ. 211 (1), 1–7.

Burton, E.A., Walter, L.M., 1987. Relative precipitation rates of aragonite and Mg calcite from seawater: temperature or carbonate ion control? Geology 15, 111–114.

Caldas, L.H., Stattegger, K., Vital, H., 2006. Holocene sea-level history: evidence from coastal sediments of the northern Rio Grande do Norte coast, NE Brazil. Mar. Geol. 228, 39–53.

Calvet, F., Cabrera, M.C., Carracedo, J.C., Mangas, J., Pérez-Torrado, F.J., Recio, C., Travé, A., 2003. Beachrocks from the island of La Palma (Canary Islands, Spain). Mar. Geol. 197 (1), 75–93.

Casella, E., Rovere, A., Pedroncini, A., Mucerino, L., Casella, M., Cusati, L.A., Vacchi, M., Ferrari, M., Firpo, M., 2014. Study of wave runup using numerical models and low-altitude aerial photogrammetry: a tool for coastal management. Estuar. Coast. Shelf Sci. 149, 160–167.

Cawthra, H., Uken, R., 2012. Modern beachrock in Durban, KwaZulu-Natal. Afr. J. Sci. 108 (7/8). http://dx.doi.org/10.4102/sajs.v108i7/8.935 (Art. #935, 5 pp.).

Cawthra, H.C., Uken, R., Ovechkina, M.N., 2012. New insights into the geological evolution of the Durban Bluff and adjacent Blood Reef, South Africa. S. Afr. J. Geol. 115 (3), 291–308.

Cooper, J.A.G., 1991. Beachrock formation in low latitudes: implications for coastal evolutionary models. Mar. Geol. 98, 145–154.

Davis, L.J., Annan, A.P., 1989. Ground-penetrating radar for high-resolution mapping of soil and rock stratigraphy. Geophys. Prospect. 37, 531–551.

Desruelles, S., Fouache, E., Ciner, A., Dalongeville, R., Pavlopoulos, K., Kosun, E., Coquinot, Y., Potdevin, J.-L., 2009. Beachrocks and sea level changes since Middle Holocene: comparison between the insular group of Mykonos–Delos–Rhenia (Cyclades, Greece) and the southern coast of Turkey. Glob. Planet. Chang. 66, 19–33.

Dunham, R.J., 1970. Keystone vugs in carbonate beach deposits. Bull. Am. Assoc. Pet. Geol. 45, 845.

El Sayed, M.K.H., 1988. Beachrock cementation in Alexandria, Egypy. Mar. Geol. 80, 29–35.

Erginal, A.E., 2012. Beachrock as evidence of sea-level lowstand during the classical period, Parion antique city, Marmara Sea, Turkey. Geodin. Acta 25 (1–2), 96–103.

Erginal, A.E., Ekinci, Y.L., Demirci, A., Bozcu, M., Ozturk, M.Z., Avioglu, M., Oztura, E., 2013. First record of beachrock on Black Sea coast of Turkey: implications for Late Holocene sea-level fluctuations. Sediment. Geol. 294, 294–302.

Fuzhi, B., Youshen, Y., 1988. Study on the "beachrock field" in Haishan Island, Guangdong Province. Chin. J. Oceanol. Limnol. 6 (4), 343–357.

Galbraith, R.F., Roberts, R.G., 2012. Statistical aspects of equivalent dose and error calculation and display in OSL dating: an overview and some recommendations. Quat. Geochronol. 11, 1–27.

Gardner, J.V., Calder, B.R., Hughes Clark, J.E., Mayer, L.A., Elston, G., Rzhanov, Y., 2007. Drowned shelf-edge deltas, barrier islands and related features along the outer continental shelf north of the head of De Soto Canyon, NE Gulf of Mexico. Geomorphology 89, 370–390.

Gehrels, R., Long, A., 2008. Sea level is not level: the case for a new approach to predicting UK sea-level rise. Geography 93, 11–16.

Ghandour, I.M., Al-Washmi, H.A., Bantan, R.A., Gadallah, M.M., 2014. Petrographical and petrophysical characteristics of asynchronous beachrocks along Al-Shoaiba Coast, Red Sea, Saudi Arabia. Arab. J. Geosci. 7, 355–365.

Gischler, E., Lomando, A.J., 1997. Holocene cemented beach deposit in Belize. Sediment. Geol. 110, 277–297.

Green, A.N., Cooper, J.A.G., Saltzmann, L., 2014. Geomorphic and stratigraphic signals of postglacial meltwater pulses on continental shelves. Geology 42, 151–154.

Hanor, J.S., 1978. Precipitation of beachrock cements: mixing of marine and meteoric waters vs. CO_2-degassing. J. Sediment. Petrol. 48, 489–501.

Hemming, N.G., Meyers, W.J., Grams, J.C., 1989. Cathodoluminescence in diagenetic calcites: the roles of Fe and Mn as deduced from electron probe and spectrophotometric measurements. J. Sediment. Petrol. 59, 404–411.

Holail, H., Rashed, M., 1992. Stable isotopic composition of carbonate-cemented recent beachrock along the Mediterranean and the Red Sea coasts of Egypt. Mar. Geol. 106, 141–148.

Hopley, D., 1986. Beachrock as a sea-level indicator. In: Van de Plassche, O. (Ed.), Sea-level Research: A Manual for the Collection and Evaluation of Data. Geo Books, Norwich, pp. 157–173.

Jarrett, B.D., Hine, A.C., Halley, R.B., Naar, D.F., Locker, S.D., Neumann, A.C., Twichell, D., Hu, C., Donahue, B.T., Jaap, W.C., Palandro, D., Ciembronowicz, K., 2005. Strange bedfellows—a deep-water hermatypic coral reef superimposed on a drowned barrier island; southern Pulley Ridge, SW Florida platform margin. Mar. Geol. 214, 295–307.

Kaufman, A., Broecker, W.S., Ku, T.L., Thurber, D.L., 1971. The status of U-series methods of mollusc dating. Geochim. Cosmochim. Acta 35, 1115–1183.

Kelletat, D., 2006. Beachrock as sea-level indicator? Remarks from a geomorphological point of view. J. Coast. Res. 22, 1555–1564.

Kindler, P., Bain, R.J., 1993. Submerged Upper Holocene beachrock on San Salvador Island, Bahamas: implications for recent sea-level history. Geol. Rundsch. 82 (2), 241–247.

Knight, J., 2007. Beachrock reconsidered. Discussion of: Kelletat, D., 2006. Beachrock as sea-level indicator? Remarks from a geomorphological point of view. Journal of Coastal Research, 22(6), 1558–1564. J. Coast. Res. 234, 1074–1078.

Koster, B., Hoffmann, G., Grützner, C., Reicherter, K., 2014. Ground penetrating radar facies of inferred tsunami deposits on the shores of the Arabian Sea (Northern Indian Ocean). Mar. Geol. 351, 13–34.

Lambeck, K., Antonioli, F., Purcell, A., Silenzi, S., 2004. Sea-level change along the Italian coast for the past 10,000 yr. Quat. Sci. Rev. 1567–1598.

Leeder, M.R., McNeill, L.C., Collier, R.E.L.1, Portman, C., Rowe, P.J., Andrews, J.E., Gawthorpe, R.L., 2003. Corinth rift margin uplift: new evidence from Later Quaternary marine shorelines. Geophys. Res. Lett. 30 (12), 1611. http://dx.doi.org/10.1029/2003GL017382.

Leeuw, G., Neele, F.P., Hill, M., Smith, M.H., Vignati, E., 2000. Production of sea spray aerosol in the surf zone. J. Geophys. Res. Atmos. (1984–2012) 105 (D24), 29397–29409.

Livsey, D., Simms, A.R., 2013. Holocene sea-level change derived from microbial mats. Geology 41, 971–974.

Locker, S.D., Hine, A.C., Tedesco, L.P., Shinn, E.A., 1996. Magnitude and timing of episodic sea-level rise during the last deglaciation. Geology 24, 827–830.

Mauz, B., Antonioli, F., 2009. Comment on "Sea level and climate changes during OIS 5e in the western Mediterranean" by T. Bardají, J.L. Goy, J.L., C. Zazo, C. Hillaire-Marcel, C.J. Dabrio, A. Cabero, B. Ghaleb, P.G. Silva, J. Lario, Geomorphology 104 (2009). Geomorphology 110, 227–230.

Meyers, W.J., 1974. Carbonate cement stratigraphy of the Lake Valley Formation (Mississippian) Sacromento Mountains, New Mexico. J. Sediment. Petrol. 44, 837–861.

Meyers, W.J., 1987. Marine vadose beachrock cementation by cryptocrystalline magnesian calcite — Maui, Hawaii. J. Sediment. Petrol. 57, 558–570.

Michelli, M., 2008. Sea-level changes, coastal evolution and paleoceanography of coastal waters in SE-Vietnam since the mid-Holocene. (Ph.D. Thesis), Christian-Albrechts-Universität Kiel, Germany (159 pp.).

Milliman, J.D., Gastner, M., Müller, J., 1971. Utilization of magnesium in coralline algae. Geol. Soc. Am. Bull. 82, 573–580.

Mills, H., Kirby, J., Holgate, S., Plater, A., 2013. The distribution of contemporary saltmarsh foraminifera in a macrotidal estuary: an assessment of their viability for sea-level studies. J. Ecosyst. Ecogr. 3, 131–147.

Mitrovica, J.X., Tamisiea, M.E., Ivins, E.R., Vermeersen, L.L.A., Milne, G.A., Lambeck, K., 2010. Surface mass loading on a dynamic earth: complexity and contamination in the geodetic analysis of global sea-level trends. In: Church, J.A., et al. (Eds.), Understanding Sea-level Rise and Variability. Blackwell Publishing Ltd, pp. 285–385.

Morhange, C., Pirazzoli, P., 2005. Mid-Holocene emergence of southern Tunisian coasts. Mar. Geol. 220, 205–213.

Montaggioni, L.F., 2005. History of Indo-Pacific coral reef systems since the last glaciation: development patterns and controlling factors. Earth Sci. Rev. 71, 1–75.

Moore, C.H., 1973. Intertidal carbonate cementation, Grand Cayman, West Indies. J. Sediment. Petrol. 43, 591–602.

Morse, J.W., Mackenzie, F.T., 1990. Geochemistry of sedimentary carbonates. Developments in Sedimentology 48. Elsevier (707 pp.).

Nathan, R.P., Mauz, B., 2008. On the dose-rate estimate of carbonate-rich sediments for trapped charge dating. Radiat. Meas. 43, 14–25.

Neal, A., 2004. Ground-penetrating radar and its use in sedimentology: principles, problems and progress. Earth Sci. Rev. 66, 261–330.

Neumeier, U., 1998. Experimental modelling of beachrock cementation under microbial influence. Sediment. Geol. 126, 35–46.

Nicolls, R.J., Cazenave, A., 2010. Sea-level rise and its impact on coastal zones. Science 328, 1517–1520.

Perry, C.T., Smithers, S.G., 2011. Cycles of coral reef 'turn-on', rapid growth and 'turn-off' over the past 8500 years: a context for understanding modern ecological states and trajectories. Glob. Chang. Biol. 17, 76–86.

Plummer, L.N., 1975. Mixing of sea water with calcium carbonate ground water. Geol. Soc. Am. Mem. 142, 219–236.

Ramsay, P.J., 1995. 9000 years of sea-level change along the southern African coastline. Quat. Int. 31, 71–75.

Ramsay, P.J., Cooper, J.A.G., 2002. Late Quaternary sea-level change in South Africa. Quat. Res. 57, 82–90.

Rey, D., Rubio, B., Bernabeu, A.M., Vilas, F., 2004. Formation, exposure, and evolution of a high-latitude beachrock in the intertidal zone of the Corrubedo complex (Ria de Arousa, Galicia, NW Spain). Sediment. Geol. 169, 93–105.

Rovere, A., Parravicini, V., Vacchi, M., Montefalcone, M., Morri, C., Bianchi, C.N., Firpo, M., 2010. Geo-environmental cartography of the marine protected area "Isola di Bergeggi"(Liguria, NW Mediterranean Sea). J. Maps 6, 505–519.

Rovere, A., Raymo, M.E., Mitrovica, J.X., Hearty, P.J., O'Leary, M.J., Inglis, J.D., 2014. The Mid-Pliocene sea-level conundrum: glacial isostasy, eustasy and dynamic topography. Earth Planet. Sci. Lett. 387, 27–33.

Sammari, C., Koutitonsky, V.G., Moussa, M., 2006. Sea level variability and tidal resonance in the Gulf of Gabès, Tunisia. Cont. Shelf Res. 26, 338–350.

Shen, J.W., Long, J.P., Pedoja, K., Yang, H.Q., Xu, H.L., Sun, J.L., 2013. Holocene coquina beachrock from Haishan Island, east coast of Guangdong Province, China. Quat. Int. 310, 199–212.

Shennan, I., 1986. Flandrian sea-level changes in the Fenland. II: tendencies of sea-level movement, altitudinal changes, and local and regional factors. J. Quat. Sci. 1, 155–179.

Siesser, W.G., 1974. Relict and recent beachrock from southern Africa. Geol. Soc. Am. Bull. 85, 1849–1854.

Spurgeon, D., Davis Jr., R.A., Shinnu, E.A., 2003. Formation of 'Beach Rock' at Siesta Key, Florida and its influence on barrier island development. Mar. Geol. 200, 19–29.

Stattegger, K., Tjallingii, R., Saito, Y., Michelli, M., Thanh, N.T., Wetzel, A., 2013. Mid to late Holocene sea-level reconstruction of southeast Vietnam using beachrock and beach-ridge deposits. Glob. Planet. Chang. 110, 214–222.

Stoddart, D.R., Cann, J.R., 1965. Nature and origin of beach rock. J. Sediment. Petrol. 35, 243–247.

Strasser, A., Davaud, E., 1986. Formation of Holocene limestone sequences by progradation, cementation, and erosion. Two examples from the Bahamas. J. Sediment. Petrol. 56, 422–428.

Strasser, A., Davaud, E., Jedoui, Y., 1989. Carbonate cements in Holocene beachrock: example from Bahiret el Biban, southeastern Tunisia. Sediment. Geol. 62, 89–100.

Ten Have, T., Heijnen, W., 1985. Cathodoluminescene activation and zonation in carbonate rocks: an experimental approach. Geol. Mijnb. 64, 297–310.

Thomas, P.J., 2009. Luminescence dating of beachrock in th southeast coast of India — potential for Holocene shoreline reconstruction. J. Coast. Res. 25, 1–7.

Vacchi, M., Rovere, A., Zouros, N., Desruelles, S., Caron, V., Firpo, M., 2012a. Spatial distribution of sea-level markers on Lesvos Island (NE Aegean Sea): evidence of differential relative sea-level changes and the neotectonic implications. Geomorphology 159–160, 50–62.

Vacchi, M., Rovere, A., Schiaffino, C.F., Ferrari, M., 2012b. Monitoring the effectiveness of re-establishing beaches artificially: methodological and practical insights into the use of video transects and SCUBA-operated coring devices. Underw. Technol. J. Soc. Underw. Technol. 30, 201–206.

van de Plassche, O., 1986. Sea-level Research: A Manual for the Collection and Evaluation of Data. Geo Books, Norwich, pp. 157–173.

Vieira, M.M., De Ros, L.F., Bezerra, F.H.R., 2007. Lithofaciology and palaeoenvironmental analysis of Holocene beachrocks in northeastern Brazil. J. Coast. Res. 23, 1535–1548.

Vousdoukas, M.I., Velegrakis, A.F., Plomaritis, T.A., 2007. Beachrock occurrence, characteristics, formation mechanisms and impacts. Earth Sci. Rev. 85, 23–46.

Walter, L.M., Hanor, J.S., 1979. Orthophosphate: effect on the relative stability of aragonite and magnesian calcite during early diagenesis. J. Sediment. Petrol. 49, 937–944.

Yaltirak, C., Sakinç, M., Aksu, A.E., Hiscott, R.N., Galleb, B., Ulgen, U.B., 2002. Late Pleistocene uplift history along the southwestern Marmara Sea determined from raised coastal deposits and global sea-level variations. Mar. Geol. 190, 283–305.